

# Anomalous Propagation of Long-Period Ground Motions Recorded in Tokyo during the 23 October 2004 $M_w$ 6.6 Niigata-ken Chuetsu, Japan, Earthquake

by Takashi Furumura and Toshihiko Hayakawa

**Abstract** Unusually large ( $>5$  cm) and prolonged shaking associated with long-period ground motions at periods of about 7 sec were observed in central Tokyo during the  $M_w$  6.6 Niigata-ken Chuetsu earthquake of 23 October 2004. The long-period ground motions caused significant resonance in high-rise buildings of about 70 floors in height. Thus, it is an urgent matter to understand the development and amplification properties of long-period ground motions in Tokyo associated with large earthquakes.

In this study, we use numerous waveform records from 585 stations in a nationwide accelerometer network (K-NET, KiK-net) and 495 intensity meters in the area around Tokyo. The data reveal that the long-period ground motion is characterized in most part by a surface, Rayleigh wave generated at the northern edge of Kanto basin, and the surface wave is developed as propagating through a thick cover of sediments ( $>3000$ – $4000$  m) that overlies rigid bedrock.

To complement the observational data, we conducted a large-scale computer simulation of seismic-wave propagation by employing the Earth Simulator supercomputer with a detailed source-slip model and a high-resolution 3D sedimentary structural model of central Japan. The results of the computer simulation demonstrate that the anomalously prolonged ground shaking of the long-period signal recorded in the center of Tokyo occurred because of the stagnation of seismic energy resulting from the multipathing and focusing of Rayleigh waves toward the bottom of the Kanto basin from surrounding mountain regions with interaction to the 3D basin structure.

*Online material:* Animations of long-period ground motions in Tokyo.

## Introduction

A large ( $M_w$  6.6) inland earthquake occurred at Chuetsu, Niigata, Japan, on 23 October 2004, causing significant damage along with 31 deaths and more than 2000 injured persons near the hypocentral region. The shallow ( $h = 9$  km) and large ( $>2$  m) slip on the earthquake fault plane produced a significant ground acceleration of more 1700 cm/sec/sec at Ojiya City immediately above the hypocenter, and a shaking intensity of 7 (the maximum on the scale of the Japanese Meteorological Agency [JMA]) was recorded in the area. This earthquake was the most damaging in Japanese modern history since the destructive Kobe ( $M_w$  6.9) earthquake of 1995.

The largest population center of Tokyo within Kanto basin is located more than 150–200 km from the earthquake epicenter, and the maximum intensity was less than 3 in this area, but Tokyo was subjected to more than 5 min of intense ( $>5$  cm) ground shaking, with a relatively long dominant

period of about 7 sec. Such large, lengthy, and long-period shaking caused significant resonance within high-rise buildings of approximately 70 floors in height, thus warning of the high risk to modern constructions posed by nearby large earthquakes.

The prolonged duration of the long-period ground motions brings to mind the severe damage and accompanying fire in large oil storage tanks that resulted from resonance associated with long-period ground motions such as those from the 1964 Niigata earthquake ( $M$  7.5) and the 1983 Central Japan Sea earthquake ( $M$  7.7) (e.g., Kudo and Sakaue, 1984). The 1985 Michoacan ( $M_w$  8.1) earthquake in Mexico resulted in more than 20,000 fatalities in Mexico City, 400 km from the epicenter, because of the effects of relatively long-period motions of 2–3 sec and an extremely prolonged duration of more than 10 min (e.g., Anderson *et al.*, 1986). A similar disaster occurred for oil storage tanks lo-

cated at Tomakomai during the 2003 Tokachi-oki  $M_w$  8.0 earthquake, even though the tanks were located more than 250 km from the epicenter (Hatayama *et al.*, 2004; Koketsu *et al.*, 2005). These examples highlight the danger of long-period motions related to large distant earthquakes.

It is therefore an urgent matter to explore the generation and development processes of long-period ground motions within Kanto basin and the propagation properties toward central Tokyo to mitigate potential disasters associated with future large earthquakes.

Ground motions associated with the Chuetsu earthquake were well characterized by recordings from a dense, nationwide strong-motion network (K-NET and KiK-net) that is installed almost uniformly across Japan at intervals of about 20–25 km (Fig. 1). In addition to the strong-motion network, we are also able to use data from intensity meters located at city government offices and fire stations, among other sites, around Tokyo. The integrated seismic network of strong-motion instruments and intensity meters (SK-net) provides us with a detailed understanding of the nature of long-period ground motions that result from the interaction of seismic waves with the 3D subsurface structure of the Kanto basin.

To complement these observational data and gain insight into the complex seismic behavior recorded beneath

Tokyo, we used the Earth Simulator supercomputer with a high-resolution subsurface structure model of central Japan and the Kanto Basin and an appropriate source-slip model for the earthquake. The results of the computer simulation of seismic-wave propagation for the Chuetsu earthquake clearly demonstrate complicated seismic behavior within the heterogeneous 3D basin structure and the process of development of the large and prolonged long-period ground motions recorded in central Tokyo. The computer simulation also offers important insights into the excitation properties of long-period ground motions in Tokyo arising from other earthquake scenarios with varying earthquake size.

### Observed Ground Motions Associated with the 2004 Chuetsu Earthquake

Figure 2 shows ground motions resulting from the Chuetsu earthquake, as recorded by the nationwide K-NET and KiK-net strong-motion networks following the visualization procedure of the seismic waves (Furumura *et al.*, 2003; Furumura and Chen, 2004). The dense and uniform recording at intervals of about 20–25 km reveals the spatial and temporal distribution of ground motions following the earthquake, including significant resonance of long-period

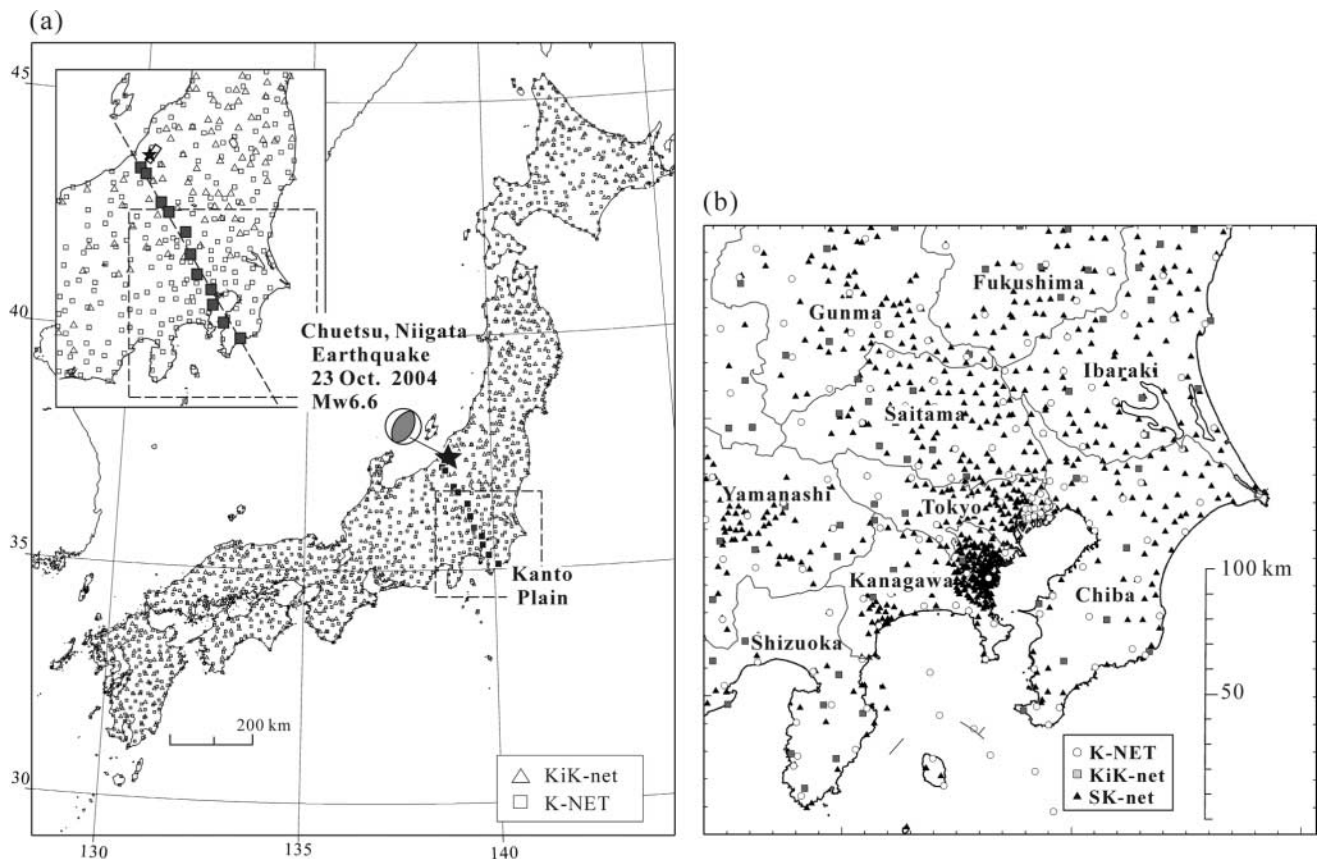


Figure 1. Distribution maps of the network of strong-motion instruments of K-NET and KiK-net (a) and intensity meters in the Kanto area (SK-net) (b). The hypocenter of the Chuetsu earthquake is shown by a star.



Figure 2. Distribution of ground motions following the Niigata-ken Chuetsu earthquake, Japan. The amplitude of the ground-velocity motions are shown for times of  $T = 20, 60, 120,$  and  $180$  sec after the earthquake rupture. (© See supplemental material in the online edition of BSSA.)

seismic waves within the thick cover of low-wavespeed sediments in locations such as Tokyo, Nagoya, and Sendai. Each of the four snapshots shown in Figure 2 is derived from the interpolation of 585 seismic records after the application of a low-pass filter ( $f < 0.5$  Hz) to reduce the spatial aliasing effect; acceleration is integrated into the ground-velocity motions to enhance the long-period ground motions greater than 1 Hz.

In the  $T = 20$  sec snapshot in Figure 2, a large ground motion resulting from the radiation of  $S$  waves from the reverse-fault source of the Chuetsu earthquake shows an almost isotropic rampart above the hypocenter. As the waves spread from the source region, the effect of near-surface heterogeneity becomes apparent (60 sec), and significant amplification of ground motions within sedimentary basins is clearly captured in the following frames at 120 and 180 sec. The reinforced long-period ground-velocity motions within thick sediments beneath central Tokyo are at least 10 times greater than those measured in surrounding areas.

In the last frame (180 sec), intense and prolonged

ground motions within the basin continued for several minutes in Kanto basin, providing a clear outline of the basin margins. Similar phenomena of amplification and prolonged ground shaking within basins are also found in other population centers such as Akita, Sendai, and Nagoya, but the effect is most pronounced within the Kanto basin.

#### Peak Ground Displacement and Intensity

Figure 3a shows the distribution of peak ground acceleration (PGA), and Figure 3b shows the peak ground displacement produced by the earthquake. A large ground acceleration in excess of 1000 cm/sec/sec is found above the source region, and the area in excess of 200 cm/sec/sec extends over a wide area of about 50 km from the hypocenter.

The PGA pattern shows an almost circular distribution above the hypocenter, with some elongation of PGA contours to the southeast (to Tokyo) and relatively large attenuation to the southwest. This pattern indicates a greater intrinsic attenuation (low  $Q$ ) in the crust of central Japan, as previ-

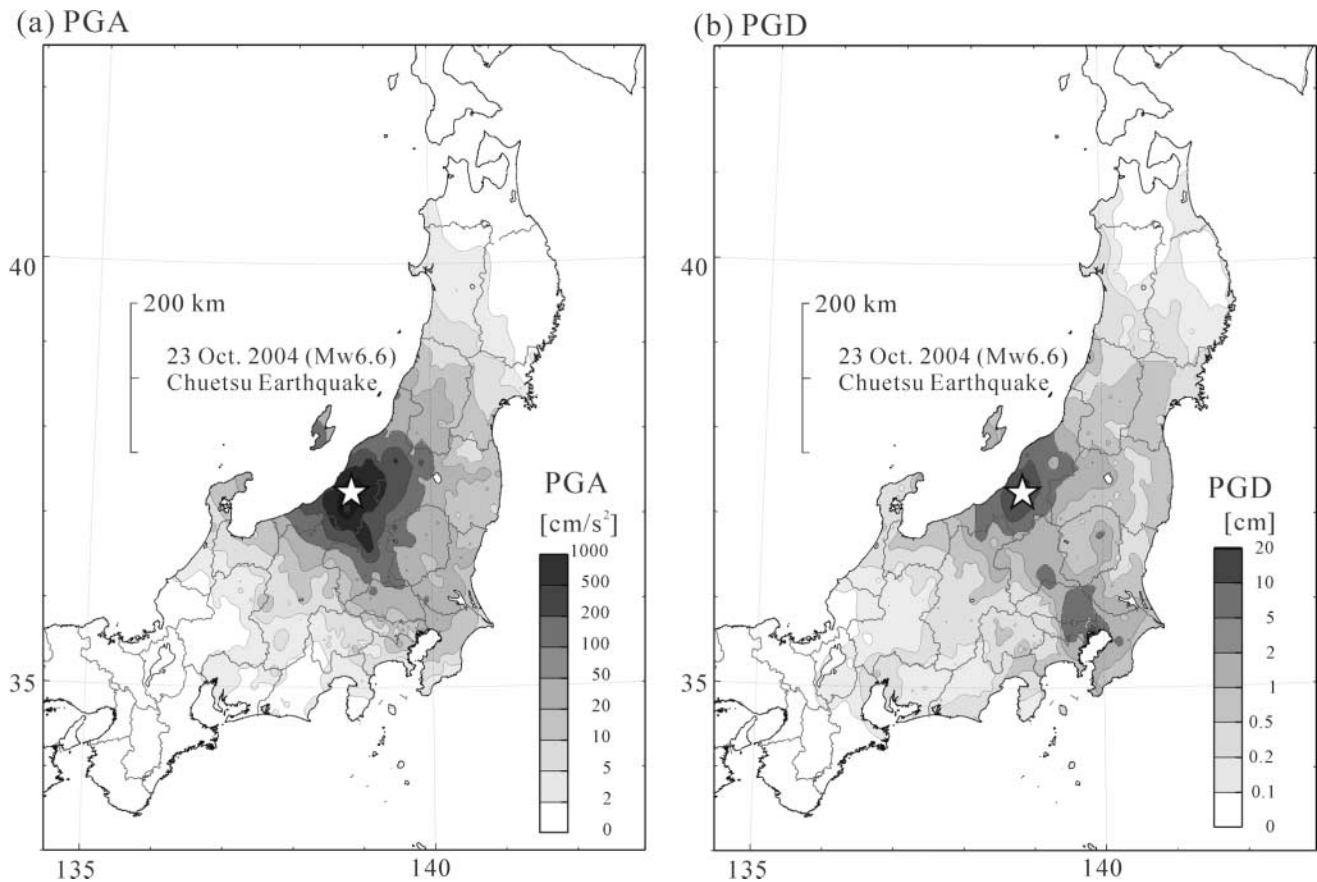


Figure 3. Distribution of peak ground acceleration (cm/sec/sec) (a) and displacement (cm) (b) during the 2004 Chuetsu earthquake, Japan.

ously discussed by many researchers on the basis of attenuation tomography (e.g., Nakamura *et al.*, 2003; Sekine *et al.*, 2005).

The attenuation and amplification properties of the long-period ground motions over about 1 sec are demonstrated by peak ground displacement (PGD), which shows a pattern somewhat different from that in the PGA map (Fig. 3a). The extension of isoseismic contours to Tokyo is clearly evident in the PGD map (Fig. 3b). This extension occurs because the radiation pattern of the *SV* wave from the reverse-fault source of the Chuetsu event is enhanced in the long-period band over 2 sec, whereas it is almost isoseismic in the short-period band less than about 0.5 sec (e.g., see Liu and Helmberger, 1985). The larger PGD recorded in the Kanto basin is also due to the strong amplification of long-period ground motions as the *S* waves enter the thick sedimentary basin. The large displacement in excess of 5 cm recorded in central Tokyo is almost comparable to the value recorded near the hypocenter.

The anomalous amplification of ground motion in central Tokyo in the relatively long-period band is clearly confirmed by comparing the peak ground velocity (PGV) observed at stations located within the basin with the amplifications predicted from a standard attenuation func-

tion for inland earthquakes in Japan (Shi and Midorikawa, 1999a, b). Most of the stations within the basin of Kanto recorded PGV values that were 2 to 10 times larger than those recorded at stations outside the basin and those predicted by the standard attenuation function for a  $M_w$  6.6 inland earthquake (Fig. 4).

#### Wave Propagation from Chuetsu to Tokyo

To study the wave-propagation characteristics from the source to the Kanto basin and the development of long-period ground motions in central Tokyo (Fig. 5), we analyzed a linearly aligned seismic record of three-component velocity waveforms recorded at 11 K-NET stations distributed from the hypocenter to Chiba via central Tokyo (see Fig. 1). The waveform at each station was multiplied by epicentral distance such that geometrical attenuation for body *P* and *S* waves is almost compensated. The horizontal ground motion is rotated to radial and transverse motions to enable the extraction of the contributions of Rayleigh and Love waves from each component, respectively.

Close to the source, short-period *S* waves are the main contributor to large shaking in three-component ground motions, but within Kanto basin, the attenuation of the short-

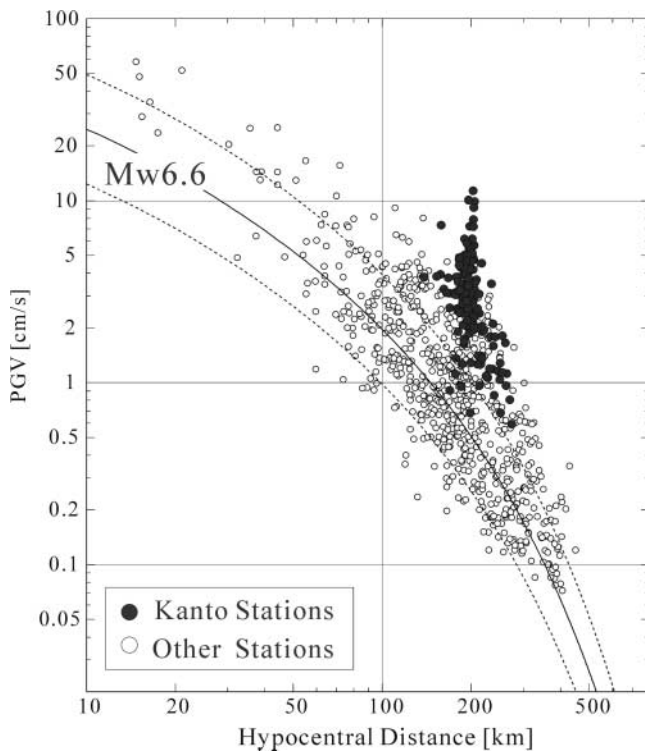


Figure 4. Attenuation of peak ground velocity as a function of hypocentral distance. Solid and dashed lines represent the expected PGV attenuation function for a  $M_w$  6.6 inland earthquake in Japan (Shi and Midorikawa, 1999a, b) and the magnification of such attenuation by factors of 0.5 and 2.0, respectively.

period  $S$  waves are significant and long-period Love and Rayleigh waves make the principle contribution to the observed large and prolonged ground motions, as depicted in the later snapshot-frames in Figure 2.

It is apparent from Figure 5 that the surface waves develop at the northern margin of the Kanto Plain, induced by conversion from  $S$  waves, and that surface waves propagate into the center of the basin at group velocity of less than 1 km/sec. The dominant periods of long-period surface waves in the center of the Kanto basin are largely consistent in the period range of 6–7 sec. The wavetrain of the surface wave is gradually elongated with propagation through the basin due to the dispersion of surface waves in the low-wave-speed basin sediments ( $V_s < 0.5$ –1 km/sec) that overlie high-wave-speed bedrock ( $V_s > 2$ –3 km/sec).

#### Predominant Period of Surface Waves

Figure 6 illustrates the velocity-response spectrum of horizontal ground motions recorded at stations in central Tokyo (TKY007) and central Chiba (CHBH10), assuming a damping coefficient of  $h = 0.05$ . A sharp resonance is expected in the relatively long-period range of about 6–8 sec, with a maximum amplitude of 16 cm/sec at TKY007 and 11 cm/sec at CHBH10. This is consistent with reports that

during the Chuetsu earthquake significant resonance occurred in tall buildings of about 70 floors (about 350 m) in height located within central Tokyo. A significant drop in the response amplitude in the short-period band below 3 sec indicates that the effect of ground motions is relatively mild in Japanese low-rise buildings of less than about 30 floors (about 150 m in height; see e.g., Architectural Institute of Japan, 2000).

Figure 7a shows the predominant period of long-period ground motions in terms of the peak resonant period of the velocity-response spectrum of horizontal ground motions observed at 495 K-NET and KiK-net stations in the Kanto area during the Chuetsu earthquake. Most of Kanto Plain recorded a peak response period of about 7 sec, and the resonance period decreases to a shorter period range of 3 sec approaching the basin margin (Fig. 7a). Thus, we observe a rough correlation between response period and the thickness of basin sediment (Fig. 7b) (Tanaka *et al.*, 2006).

Sediments thicker than 4000 m beneath CHBH10 are expected to have much longer-period surface waves at a dominant period of about 10–12 sec, as observed during the southeast-off Kii Peninsula earthquake ( $M_w$  7.4) of 5 September 2004, located 400 km southwest of Tokyo. As the radiation of  $S$  waves from the large  $M_w$  7.4 earthquake contain much longer-period ground motions, the resultant ground motions in the Kanto basin should show much larger peaks in the long-period range. During the southeast-off Kii Peninsula earthquake, most Chiba stations recorded long-period surface wave of 12 sec (Hayakawa *et al.*, 2005; Miyake and Koketsu, 2005), although most aftershocks of  $M_w < 6.6$  had a resonance period similar to that of the Chuetsu earthquake (about 7 sec).

#### Development of Surface Waves in the Kanto Plain

The uniform distribution of the K-NET and KiK-net across all of Japan at intervals of about 20–25 km is very useful in understanding the regional wave field and local amplification effects within sedimentary basins (Fig. 2); however, in terms of the wavelength of the dominant period of surface waves (less than 7 km;  $T = 7$  sec and  $V_s < 1$  km/sec), the strong-motion network may be too coarse to investigate the detailed behavior of surface waves when interacting with complicated 3D basin structure shown in Figure 7b.

We therefore used data from a network of intensity meters operated by, for example, city government offices, fire stations, and JMA. Similar to K-NET and KiK-net, the intensity meters consist of three-component force-balanced accelerometers to provide a flat-response range from DC to more than 30 Hz, thus enabling them to be utilized for analyzing long-period ground motions. The integrated strong-motion network in the Kanto area (SK-net), combined with K-NET, KiK-net, and the intensity meters provides a much denser station spacing of about 2–10 km.

The propagation of seismic waves recorded by the SK-net is illustrated in Figure 8 as the particle motion of hori-

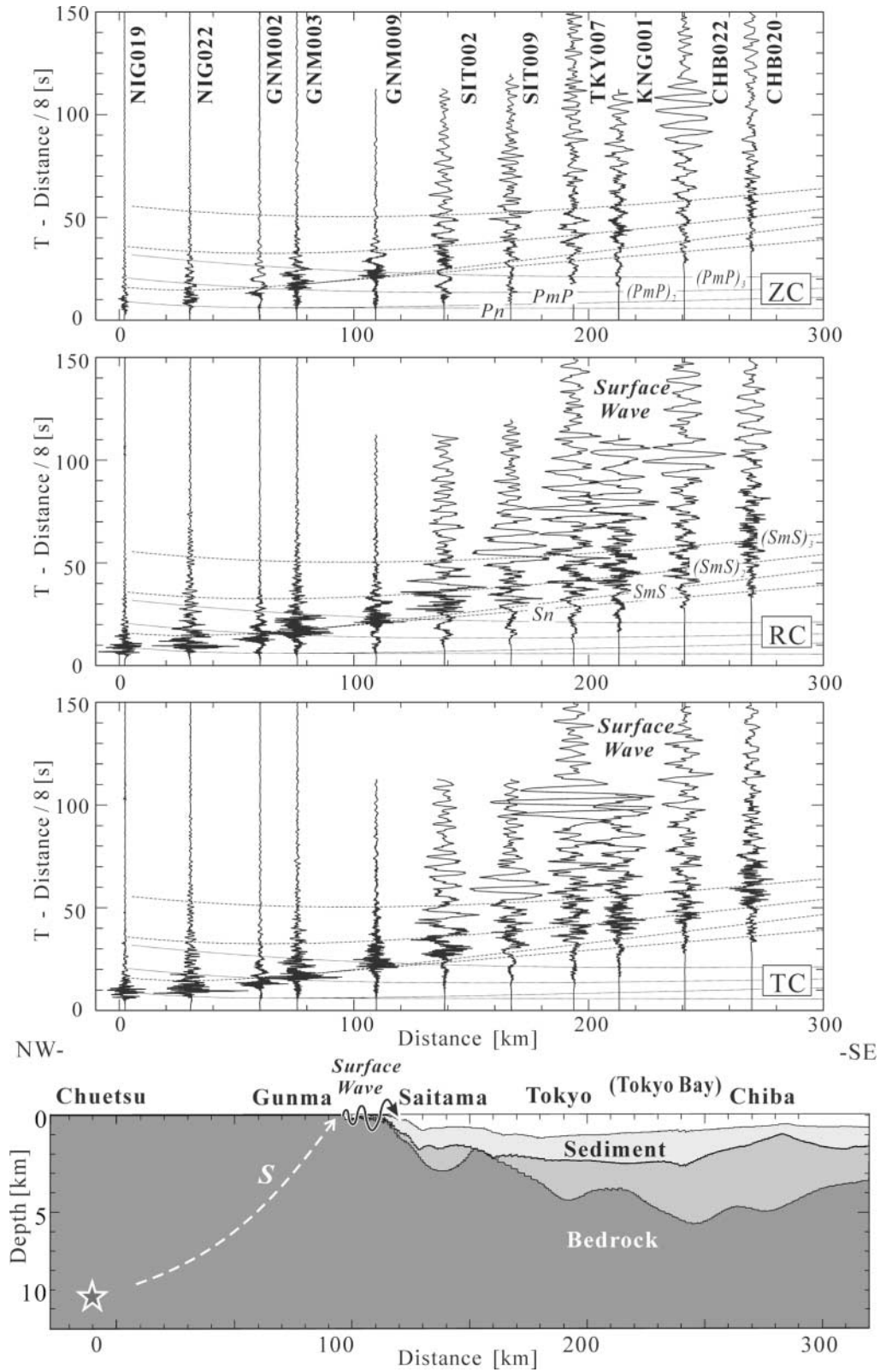


Figure 5. Three-component recorded section of ground-velocity motions of vertical (ZC), radial (RC), and transverse (TC) components associated with the Chuetsu earthquake as recorded at 11 stations from Chuetsu to Chiba (stations are shown in Fig. 1 by solid squares). The bottom panel shows a cross section of subsurface structure along the line of the stations (Tanaka *et al.*, 2006) and an interpretation of surface-wave generation at the northeastern end of Kanto basin.

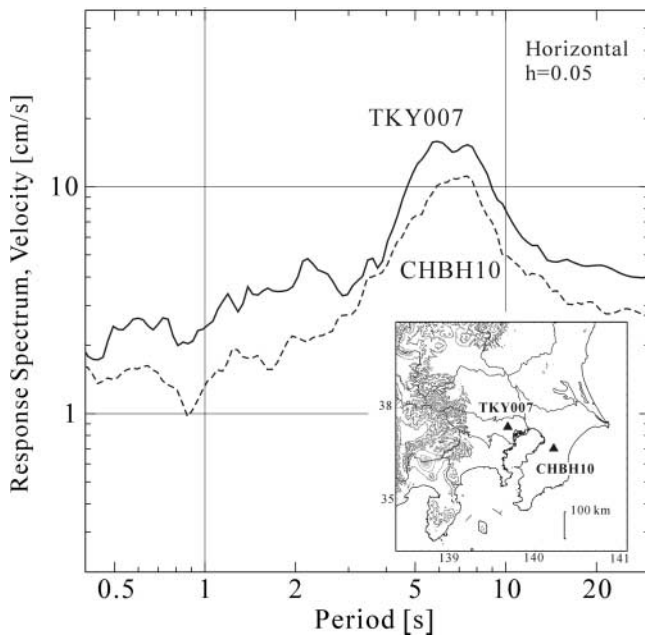


Figure 6. Velocity-response spectrum of horizontal ground motions recorded in central Tokyo (TKY007) and Chiba (CHBH10) during the Chuetsu earthquake.

zontal velocity ground motions. A bandpass filter with a cut-off period between 3.5 and 14 sec was applied to each seismogram trace to enhance the surface wave at 7 sec. The trajectory of particle motion at each time frame is illustrated in a 7-sec time window, which also enhances the polarization and propagation characteristics of the long-period surface waves. The configuration of basement topography is illustrated in Figure 8f, and is compared with the propagation and amplification characteristics of the surface waves in Figure 8a–e.

The particle motions in the first frame (Fig. 8a; 60 sec) show the development of surface waves at the boundary of the Gunma and Saitama prefectures and propagation into the center of Tokyo at a wave speed of about 1 km/sec. Particle motion is almost polarized along the wave propagation (i.e., radial) direction, confirming that Rayleigh waves are the dominant component of the large ground motion recorded in the Kanto basin during the Chuetsu earthquake. Amplification and elongation of ground motion as the surface waves approach central Tokyo is clearly seen in the 70-sec frame.

In the middle frame (Fig. 8b; 70 sec), a family of large surface waves is seen to be propagating along the western margin of the Kanto basin in the direction of Kanagawa along a steep basin wall. The waves suddenly change direction to head toward central Tokyo as they drop from the steep slope of the bedrock interface to the deep basin bottom (Fig. 8d, 105 sec).

Thick (>3000 m) and low-wave-speed ( $V_s = 0.5$ – $1.7$  km/sec) sediments beneath Tokyo attract surface waves

from outer high-wave-speed ( $V_s > 2.4$  km/sec) regions, as the propagation speed of the 7-sec surface wave is primarily controlled by the superficial layer of depths of 2000–7000 m.

In the last frame (Fig. 8e; 135 sec), the two sets of surface waves, one propagating directly from the north and the other rerouting from the area to the west of Tokyo, converge in central Tokyo. The merging of the two surface waves results in intense and prolonged ground shaking in the center of Tokyo, as observed in Figures 2 and 5. It is also apparent that the large later signals depicted in the transverse motion of TKY007 (Fig. 5) are not Love waves but are in fact Rayleigh waves, as the signal oscillates in a radial direction when passing the stations from east to west.

Such rerouting of the surface waves, first propagating along the western margin of the Kanto basin and then to the center of Tokyo, has previously been documented following shallow earthquakes that occurred near Izu Peninsula, southwest of Tokyo (e.g., Kinoshita *et al.*, 1992; Koketsu and Kikuchi, 2000; Miura and Midorikawa, 2001; Yamada and Yamanaka, 2003). The reported observations associated with the Chuetsu earthquake northwest of Tokyo indicate that such an anomalous propagation of surface waves and significant elongation and amplification of ground motions in central Tokyo are likely to be common characteristics of all shallow earthquakes that occur in the area southwest of Tokyo.

### Computer Simulation of the Chuetsu Earthquake

The dense seismic observations from the nationwide strong-motion network and the network of intensity meters provide clear visualization of the seismic wave field in the Kanto area during the Chuetsu earthquake, with an interaction in 3D sedimentary structure within the Kanto basin. However, seismic observations are restricted to land-based stations, and no seismic instrumentation is located in Tokyo Bay or on mountainsides in the area. It therefore remains difficult to understand both the propagation properties of surface waves in Tokyo Bay as the waves pass through Tokyo to Chiba and the cause of prolonged shaking during ground motions in the Tokyo Bay area.

To complement the observations described previously and gain further insight into the nature of surface waves in the Tokyo Bay area, we used the Earth Simulator supercomputer to simulate ground motions during the Chuetsu earthquake with a high-resolution subsurface structure model of central Japan (Tanaka *et al.*, 2006) and a source-slip model for the earthquake (Hikima and Koketsu, 2005).

### Subsurface Structural Model

The simulation model covers an area of  $440 \times 250$  km to a depth of 160 km, and is discretized by a small mesh size of  $0.2 \times 0.2 \times 0.1$  km for depths less than 10 km and a double-sized grid ( $0.4 \times 0.4 \times 0.2$  km) for deeper areas of 10–160 km depth.

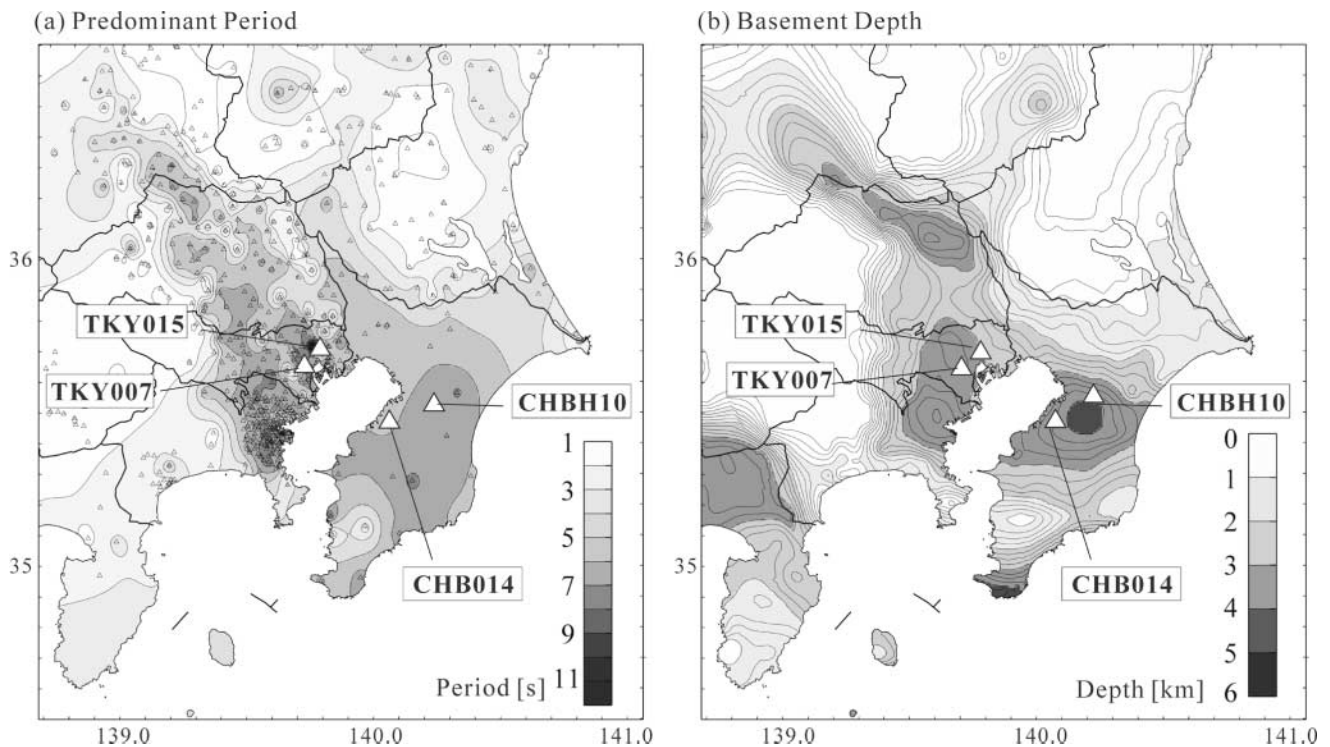


Figure 7. (a) Dominant period of surface waves in the Kanto region during the Chuetsu earthquake, and (b) topography of basement within Kanto basin (Tanaka *et al.*, 2006).

The 3D subsurface structural model of sedimentary structure covering the area from Chuetsu to Tokyo was constructed recently based on the results of several reflection and refraction experiments,  $P$ - and  $S$ -wave speed logging data from a deep borehole, array measurements of microtremor data, and Bouguer anomaly data (Tanaka *et al.*, 2006).

The 3D structure model of the sedimentary basin was constructed using three layers ( $V_s = 0.5, 1.0,$  and  $1.4$  km/sec) overlying a rigid bedrock of  $V_s = 2.9$  km/sec. The physical parameters of each layer and basement bedrock are shown in Table 1, whereas the geometry of the dominant sedimentary structure is displayed in Figure 9.

Details of the deep structure of the crust and uppermost mantle in central Japan is based on the *aki35* standard earth model (Kennett *et al.*, 1995), with a spatially varying crust-mantle (Moho) boundary and midcrustal (Conrad) interface following the results of Ryoki (1999). Attenuation coefficients for  $P$  and  $S$  waves ( $Q_p$  and  $Q_s$ ) for each sedimentary layer are based on the  $Q_s$  model obtained by Yamanaka and Yamada (2002), and we assumed that  $Q_p = 2Q_s$ .

#### Fault-Rupture Model

The fault-rupture model employed in the present simulation is derived from an inversion using KiK-net strong-motion records (Hikima and Koketsu, 2005). The fault model is represented by a  $24 \times 16$  km area with fault segments of  $2 \times 2$  km. The inferred fault segment shows a

large slip of about 2 m around the area of the hypocenter at 9 km depth, and the fault rupture runs bilaterally on the fault plane to the northeast and southwest at an average rupture speed of  $V_r = 2.8$  km/sec. To implement the source slip model in a fine simulation grid, the source model is resampled into  $0.5 \times 0.5$  km subfaults using a linear interpolation function.

Although the source time function for each subfault derived by the inversion is represented by a set of triangular functions with a time width of 1 sec, the direct application of such a smooth source time function to each segment of the resampled fault plane may underestimate high-frequency signals in excess of about 1 Hz. We therefore employed the appropriate pseudodynamic source time function of Nakamura and Miyatake (2000), which is derived empirically from a dynamic fault-rupture simulation using the slip-weakening model.

The slip-velocity function of Nakamura and Miyatake (2000) can be constructed by following physical parameters that control the dynamic properties of the fault rupture, such as the static stress drop ( $D_s$ ), maximum slip velocity ( $V_{max}$ ), rise time ( $T_r$ ), and fault-rupture sustain time ( $T_s$ ). The distribution of  $D_s$  on the fault plane can be estimated from the slip distribution ( $D$ ) of the source model derived by Hikima and Koketsu (2005) with the use of the relationship of a convolutional integral (e.g., see Guatteri *et al.*, 2004), while  $D_s$  is obtained by multiplying wavenumbers and  $D$  in the wavenumber domain:



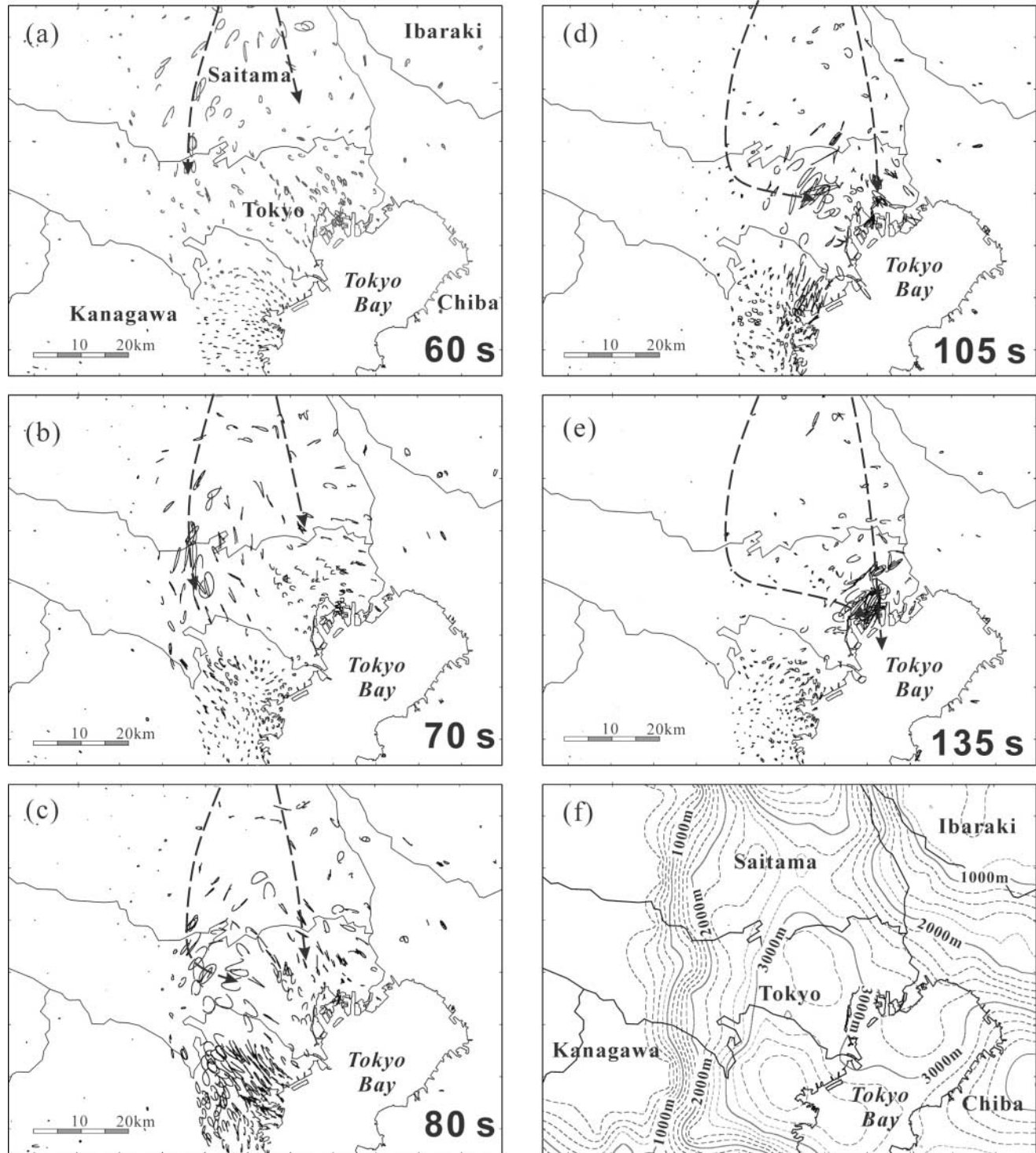


Figure 8. (a)–(e) Particle motions of horizontal ground motions recorded by 495 intensity meters stationed in Kanto basin and 176 K-NET and KiK-net stations. The pair of dashed lines in each figure represents the estimated major wave-propagation paths of the surface waves that affected central Tokyo. The time from earthquake rupture is shown in the bottom right corner of each figure. (f) Configuration of basement topography beneath Tokyo. (E See supplemental material in the online edition of BSSA.)

Table 1

Physical Parameters of  $P$ - and  $S$ -Wave Velocity, Rock Density, and Anelastic Attenuation Coefficients for Each Layer Represented in the Simulation

	$V_p$ (km/sec)	$V_s$ (km/sec)	$\rho$ ( $t/m^3$ )	$Q_p$	$Q_s$
Sedimentary layer					
Layer 1	1.8	0.5	1.9	100	50
Layer 2	2.5	1.0	2.1	200	100
Layer 3	3.1	1.4	2.1	300	150
Basement	5.5	2.9	2.6	600	300
Upper crust	5.8	3.3	2.7	700	350
Lower crust	6.5	3.7	2.7	800	400
Upper mantle	8.0	4.5	2.8	1000	500

$$D_s(k) = -K(k) * D(k),$$

where  $K(k)$  represents the static stiffness function, which for crustal earthquakes can be approximated as  $K(k) = -0.5 * \mu * k$  (Guatteri *et al.*, 2004), and  $\mu$  is rigidity. Thus, the distribution of  $D_s$  within each subfault is calculated from the inferred slip model derived from the inversion via the Fourier transform and subsequent inverse Fourier transform of  $D_s(k)$ .

Following the study of Nakamura and Miyatake (2000),  $V_{\max}$  for each subfault can be approximated using  $D_s$ , maximum frequency ( $f_{\max}$ ), width of the fault ( $w$ ), and fault rupture speed ( $V_r$ ) as:

$$V_{\max} = D_s * \sqrt{(2 * f_{\max} * w * V_r)} / \mu,$$

where we assumed  $f_{\max} = 8$  Hz. The slip rise time ( $T_r$ ) is assumed empirically from the width of the fault and the fault rupture speed as:

$$T_r = 0.5 * w / V_r,$$

and the fault rupture sustain time is  $T_s = 1.5 * T_r$ . The inferred pseudodynamic source model and examples of the slip-velocity function at each point on the fault are shown in Figure 10.

#### Parallel Finite-Difference Method (FDM) Simulation

Seismic-wave propagation was calculated by the parallel finite-difference method (FDM) using a sixteenth-order staggered-grid scheme in horizontal directions and a fourth-order scheme in the vertical direction (Furumura and Chen, 2005). The viscoelastic anelastic attenuation of frequency-independent  $Q_p$  and  $Q_s$  are incorporated in the FDM simulation using the memory variable algorithm based on Robertson *et al.* (1994). The algorithm for the parallel computing is based on the domain-partitioning procedure where the 3D model is partitioned vertically into several subregions that are assigned to many processors, and the message-passing

interface (MPI) is used to exchange data between neighboring processors.

As a minimum  $S$ -wave velocity of  $V_s = 0.5$  km/sec is assigned to the uppermost sedimentary layer, the higher-order, staggered-grid FDM simulation can accurately reproduce seismic-wave propagation for frequencies up to 1 Hz, with sampling of 2.5 and 5 grid points per shortest wavelength in the horizontal and vertical directions, respectively. Since the seismic source radiates higher-frequency seismic waves to frequencies up to  $f_{\max} = 8$  Hz, a low-pass filter was applied to the simulation results to remove high-frequency signals in excess of 1 Hz.

We used the Earth Simulator supercomputer for the parallel FDM simulation; the present simulation took 3 hours using 80 nodes (640 processors).

#### Simulation Result

Though the seismic observation is restricted in land and no seismic instruments are available in the mountain region and inside Tokyo Bay, the computer simulation enables visualization of the seismic-wave field throughout the entire Kanto region.

Figure 11 illustrates a series of six snapshots of horizontal ground-velocity motions in Kanto basin from the Chuetsu earthquake. Each frame of the snapshot clearly demonstrates the generation and complicated propagation characteristics of the long-period surface waves that interact in 3D basin structure of Kanto basin.

The simulation snapshot at 50 sec (Fig. 11a) shows the generation of surface waves at the northwestern edge of Kanto basin and significant amplification of ground motions within the thick cover of soft sediments. The simulation results at 60 sec (Fig. 11b) show rerouting of surface waves from bounding mountain side to the center of Tokyo along the western margin of the sedimentary basin and subsequent focusing toward the center of Tokyo Bay (Fig. 11c,d; 70 sec, 80 sec). The surface waves travel across Tokyo Bay to Chiba via the deepest part of the basement (Fig. 11e; 100 sec). The last snapshot (Fig. 11f; 120 sec) clearly demonstrates the stagnation of surface waves in the area around Tokyo with thick cover of deep basin sediments, like the stormy flow of the river.

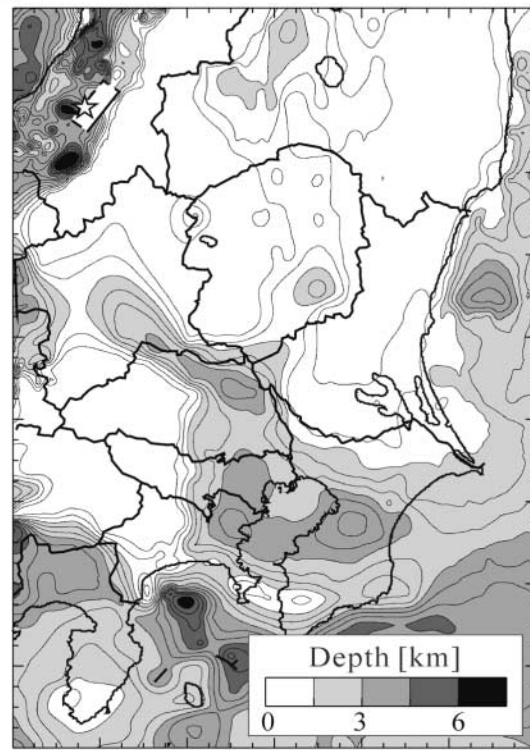
The result of the computer simulation confirms that the mortarlike shape of the sedimentary basin of Kanto basin and the thick cover of overlying sediments below Tokyo are the main causes of the large and prolonged ground shaking in Tokyo associated with long-period surface waves produced by the large earthquake. The anomalous large and long-time shaking of ground motions in Tokyo and Chiba result from the multiple reflections of seismic waves in the thick sedimentary basin associated by multipathing and focusing of surface waves toward the bottom of the Kanto basin.

We now compare simulated waveforms of three-component ground-velocity motions with observations re-

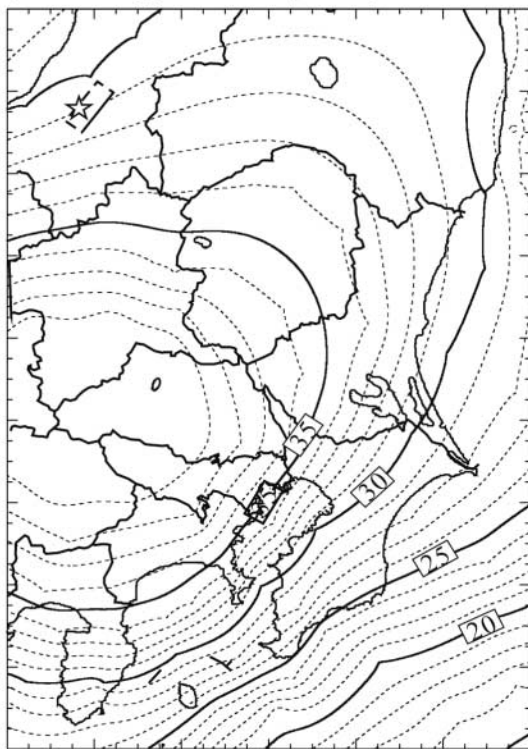
(a) Sedimentary layer2 / 3



(b) Basement



(c) Crust / Upper mantle (Moho)



(d)

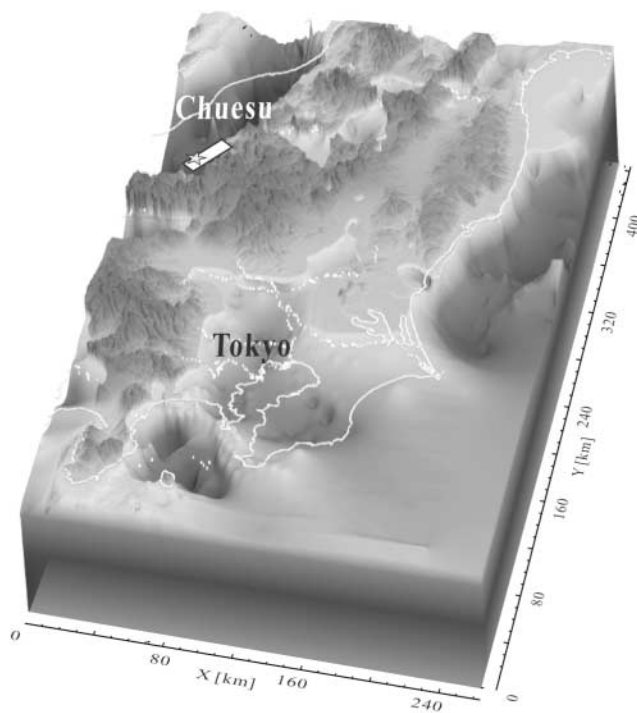


Figure 9. Structural model of central Japan used in the 3D simulation of seismic-wave propagation, showing depth distribution of sedimentary layers of layer2 ( $V_s = 1.0$  km/sec)/layer3 ( $V_s = 1.4$  km/sec) interface (a), depth distribution of basement ( $V_s = 2.9$  km/sec) (b), crust/upper-mantle (Moho) interface (c), and 3D view of the simulation model showing basement topography (d).

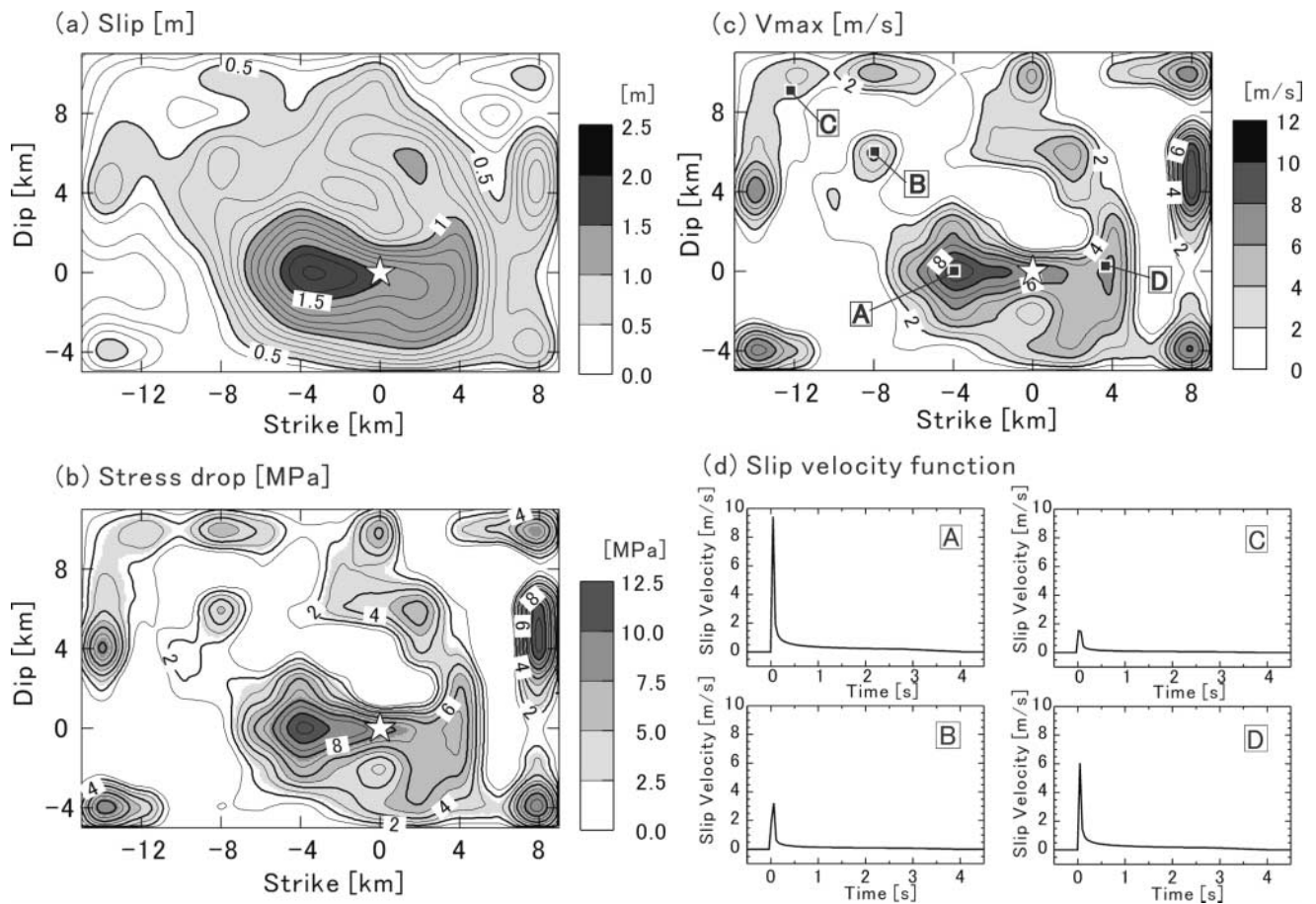


Figure 10. Pseudodynamic source model for the Chuetsu earthquake. (a) Source-slip model derived from the inversion described by Hikima and Koketsu (2005). (b) Estimated static stress drop. (c) Maximum slip velocity. (d) Examples of the pseudodynamic slip-velocity function defined at A, B, C, and D on the fault plane.

corded at stations GNM002, GNM009, SIT009, KNG001, and CHB022 within Kanto basin (Fig. 12). A low-pass filter with a cutoff frequency of 1 Hz was applied to the simulated and observed seismograms.

The simulation results demonstrate the major features of observed strong ground motions such as the dominant period of the surface waves and the shape of  $S$  and surface waves. The very large and prolonged shaking of long-period ground motions resulting from the Chuetsu earthquake across Kanto basin is well demonstrated in the simulation. Though the recordings of strong-motion instruments suddenly stop when the ground acceleration level drops below the recording level, the simulated waveforms demonstrate the very long duration of long-period signals in Kanto basin resulting from the Chuetsu earthquake.

As the present simulation does not accommodate short-period signals of  $<1$  sec, the simulation results underestimate short-period  $P$ - and  $S$ -wave signals of the earthquake, but long-period signals that develop subsequently within Kanto basin are almost comparable to the observational data. Thus, the current model of the subsurface structure of central

Japan and sedimentary basin structure of the Kanto basin and the FDM simulation technology are considered to be suitable for use in understanding the major characteristics of long-period ground motions in Tokyo resulting from large earthquakes.

## Discussion

The dense-array observations and corresponding computer simulation make it clear that the long-period surface waves are generated at the basin interfaces and develop significantly with ongoing propagation through thick sediments beneath Kanto basin. Consequently, we consider that the generation of long-period ground motions within Kanto basin is a common characteristic of all earthquakes that occur in the Chuetsu area.

However, such long-period motions were not recorded for aftershocks of the Chuetsu earthquake with magnitudes less than  $M_w$  5.8 (Fig. 11). We next examine the excitation properties of long-period surface waves in central Tokyo for different earthquakes of varying magnitude.

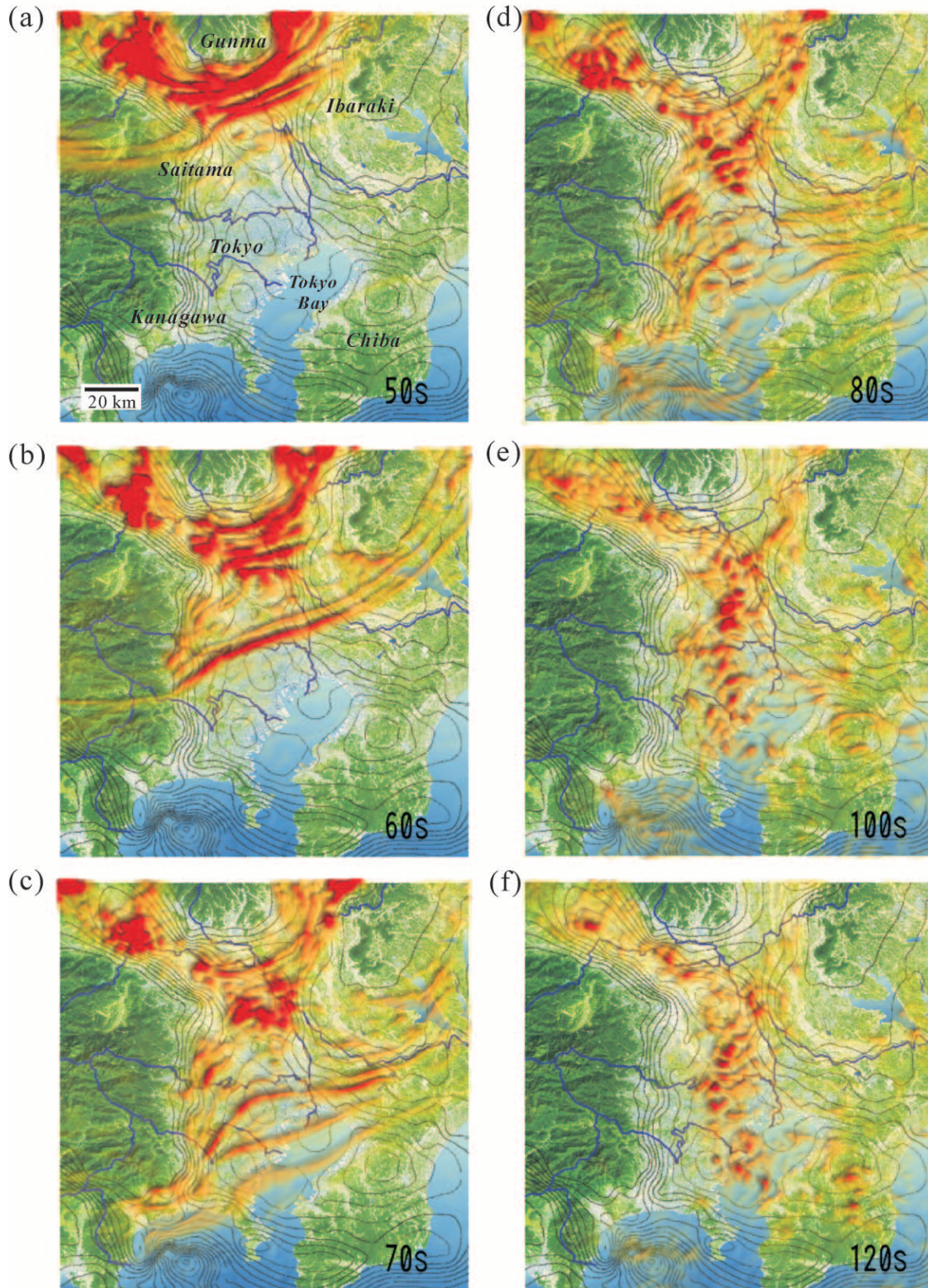


Figure 11. Simulated horizontal ground motions in Kanto basin. The time from the start of the earthquake is shown in the bottom right corner of each figure. The configuration of basement topography is also shown. Contour interval is 400 m. (© See supplemental material in the online edition of BSSA.)

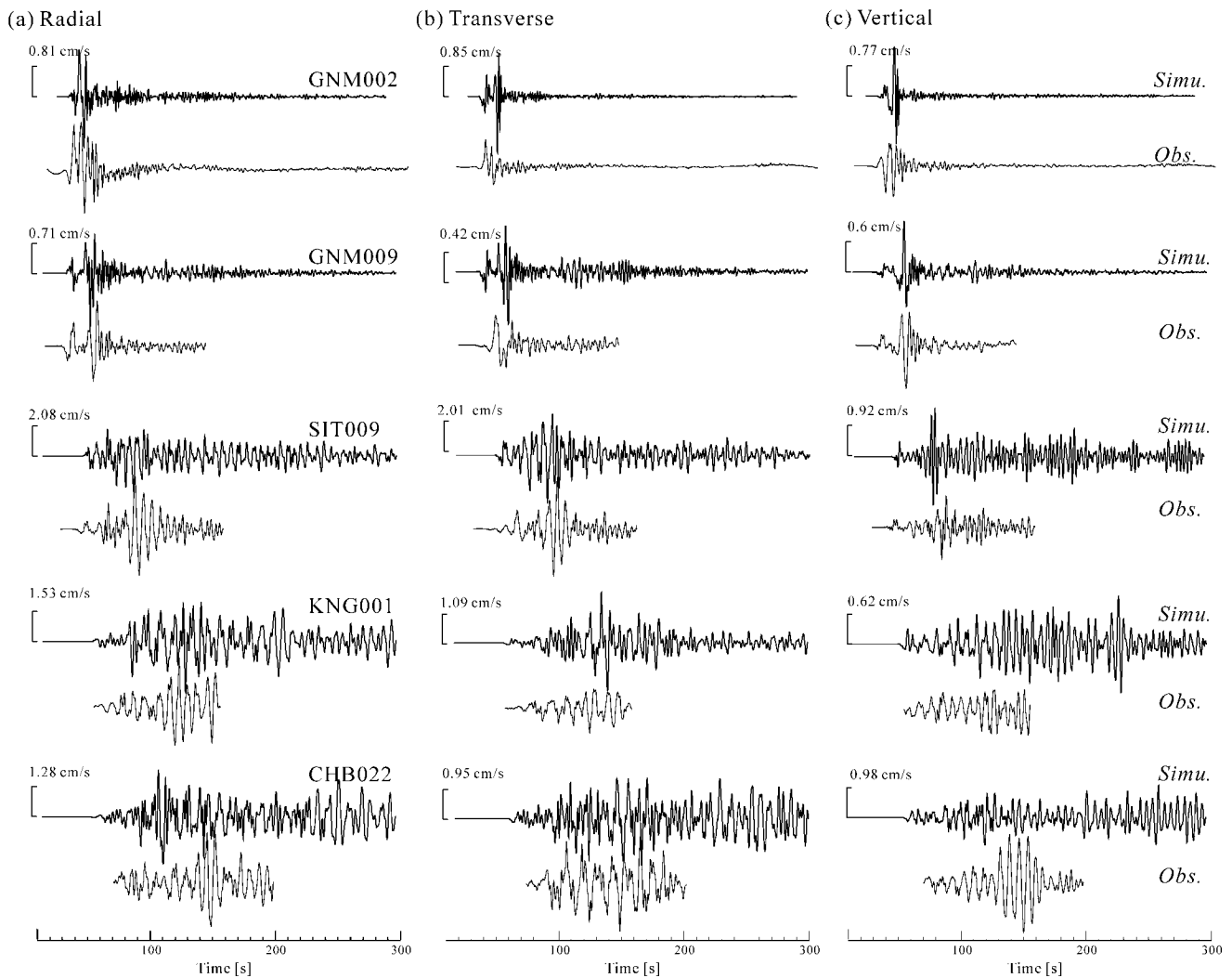


Figure 12. Comparison of simulated waveforms (thick lines) and observed waveforms (thin lines) of ground-velocity motions at five K-NET stations located close to Tokyo, for radial- (a), transverse- (b), and vertical-component (c) ground-velocity motions.

Figure 13 compares the velocity waveform recorded in central Tokyo (TKY015) (see Fig. 7) and in Chiba (CHB014) for the mainshock ( $M_w$  6.6) and three aftershocks ( $M_w$  5.8, 5.6, 5.0) of the Chuetsu earthquake, all with a similar source depth ( $h = 9\text{--}12$  km). Because the strong-motion instruments rely on an event trigger system, the ground motions of two small aftershocks ( $M_w$  5.6, 5.0) were not recorded at CHB014.

Each seismogram in Figure 13 is normalized by the amplitude of the  $S$  wave such that the relative excitation strength of the long-period surface wave, as magnitude change, can be compared. The velocity-response spectrum for each seismogram is shown in Figure 13, showing a significant drop in response at 7 sec as the magnitude decreases very clearly. For small earthquake ( $M_w < 5.6$ ) record of TKY015, the amplitude of the later surface wave is approximately one-half to one-fourth of the  $S$  wave, and the re-

sponse in the short-period band below 2 sec caused by the large  $S$  wave is more pronounced than that for the long-period surface wave in 7 sec. Larger response in the lower-period band below 1 sec for small earthquakes ( $M_w$  5.0,  $h = 11$  km) than large  $M_w$  5.6 ( $h = 14$  km) event may be due to relatively larger excitation of short-period surface waves from the shallow ( $h = 11$  km) source.

The aftershock record in CHB014 also shows no large surface wave following a short-period  $S$  wave.

Similar observations were made during the  $M_w$  7.4 southeast-off Kii Peninsula earthquake from another central Chiba station (CHBH10) where very thick sediments ( $>4000$  m) resulted in the development of much longer surface waves of about 12 sec (Hayakawa *et al.*, 2005; Miyake and Koketsu, 2005), but aftershocks of the southeast-off Kii Peninsula earthquake with magnitudes less than  $M_w$  6.8 produced much shorter-period (7 sec) surface waves (Hayakawa

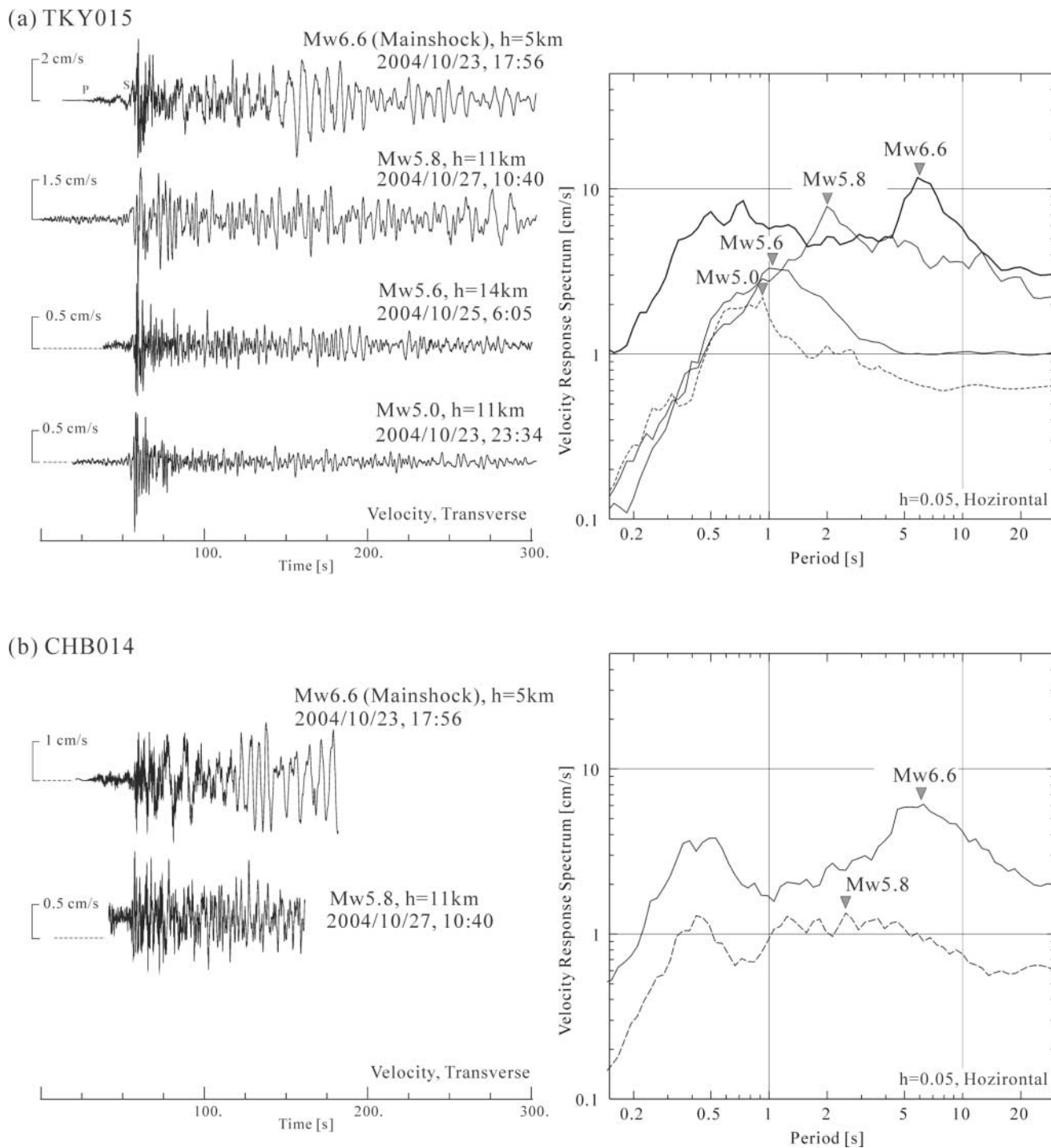


Figure 13. Comparison of observed ground motions recorded at TKY015 (a) and CHB014 (b) of the transverse component velocity motion for the mainshock and the aftershocks of the Chuetsu earthquake. The right-hand figure shows the velocity-response spectra for the mainshock and three aftershock records. Each waveform trace is normalized by the amplitude of the *S* wave. The first resonant periods are marked by triangles.

*et al.*, 2005), as apparent in Figure 6 for the  $M_w$  6.6 Chuetsu earthquake.

To demonstrate the relative excitation strength of the long-period surface waves and changes in the dominant period of surface waves with varying magnitude, we conducted a set of computer simulations using enlarged ( $M_w$  7.2) and shortened ( $M_w$  6.0, 5.4) source models by stretching and shortening the fault size of the model of the Chuetsu earthquake, respectively. We kept the existing pattern of slip distribution, source depth, and static stress drop, but the dipping angle of the  $M_w$  7.2 source is declined from 53 to 23 degrees to place the fault plane of the larger source below the surface. The source parameters for the large and small earthquakes are listed in Table 2.

Figure 14 shows a comparison of waveforms for central Tokyo (TKY015) and Chiba (CHB014) derived from simulations using a very small ( $M_w$  5.4), small ( $M_w$  6.0), and large ( $M_w$  7.2) earthquake source, compared with the corresponding simulation for the  $M_w$  6.6 Chuetsu earthquake. Excitation of the long-period surface wave is much greater for the large ( $M_w$  7.2) earthquake, and the velocity response at 8 sec is almost twice as large as that for the  $M_w$  6.6 event. For the small earthquake ( $M_w$  6.0), the drop in velocity response within the longer-period band over 7 sec is striking; large resonances occur in short-period band below 6 sec.

For the Chiba (CHB014) station located above much thickness of sediments ( $\sim 4000$  m), the shift in the peak resonant period from 6 to more than 10 sec with increasing magnitude is more pronounced, and we observe a greater response in the longer-period band of 8–12 sec during the large ( $M_w$  7.2) earthquake, as observed for the 2004 south-east-off Kii Peninsula  $M_w$  7.4 earthquake (Hayakawa *et al.*, 2005; Miyake and Koketsu, 2005).

The simulation results indicate that to make realistic predictions of long-period ground motions expected for future seismic events, we need good estimates of earthquake size (magnitude) and therefore the radiation characteristics of the long-period  $S$  wave from the earthquake fault.

## Conclusions

Large and prolonged shaking associated with long-period ground motions at periods of  $T = 7$  sec occurred in central Tokyo during the Chuetsu earthquake in 2004. Such large and shallow, inland earthquakes of more than  $M_w$  6.6 have not occurred around Tokyo since the Western Nagano

$M$  6.8,  $h = 2$  km earthquake of 1984. Thus, the observations of the destructive long-period ground motions developed by the Chuetsu earthquake are the first to record strong impacts on modern large-scale constructions in Tokyo; these observations can therefore be used to understand the potential disasters that might result from future large-scale earthquakes.

Dense-array observations from the nationwide strong-motion network (K-NET, KiK-net) combined with a network of intensity meters in the Kanto area clearly demonstrate the development of long-period ground motions via interaction with the complex structure of Kanto basin. A corresponding computer simulation using a detailed 3D model of basin structure and a source-slip model for the Chuetsu earthquake clearly demonstrates the rerouting and focusing of surface waves from bounding mountains toward central Tokyo and the subsequent stagnation of seismic energy in thick sedimentary basin cutting through central Tokyo from northwest to Tokyo Bay; this stagnation is the main cause of the prolonged and large ground shaking recorded in central Tokyo.

In this article we studied anomalous propagation and amplification characteristics of the long-period ground motions in thick sediments of Kanto basin during the Chuetsu earthquake, but the generation of the long-period ground motions within Kanto basin should be a common characteristic of all large, shallow earthquakes that occur in southwest of Tokyo.

For the computer simulation of the 2004 Chuetsu earthquake, we were able to achieve a good match with observational data for most of the dominant features of the long-period surface waves that developed in the Kanto basin. Thus, we believe that the simulation model can be applied to the understanding of the strong ground motions expected for future earthquake scenarios that might occur near Tokyo.

## Acknowledgments

We acknowledge the National Council for Disaster, Cabinet Office, Japan, for providing the subsurface structural model, and the Earth Simulator Center for their support with computer resources. CPU time on the Earth Simulator was supported by the project Multi-Scale and Multi-Physics Integrated Simulation study (CREST) of the Japan Science and Technology Agency. K-NET and KiK-net data were provided by the National Institute for Earth Science and Disaster Research, Japan. SK-net data were provided by the Earthquake Research Institute, University of Tokyo. This study was also supported by the Special Project for Earthquake Di-

Table 2  
Fault Parameters of Small and Large Earthquake Sources Synthesized from the Actual Source Model of the Chuetsu Earthquake

Source Model	Fault Size L*W (km)	$M_w$	Maximum Slip (m)	Maximum Stress Drop (MPa)	Rise Time (sec)
Very small	5.6 * 4	5.4	0.42	12	0.7
Small	11.5 * 8	6.0	0.85	12	1.4
Large	46 * 32	7.2	3.44	12	5.5
2004 Chuetsu earthquake	23 * 16	6.6	1.72	12	2.8



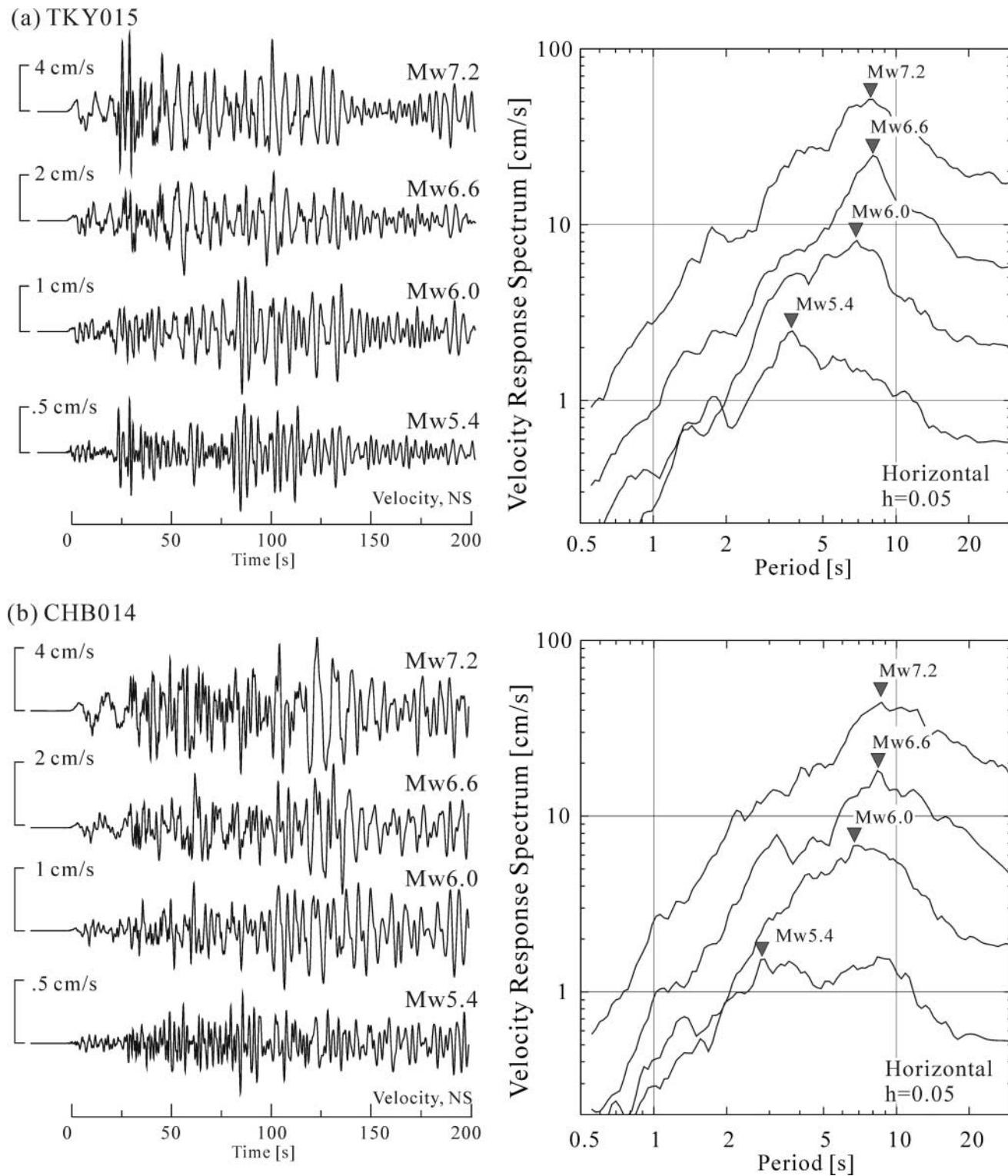


Figure 14. Comparison of simulated waveforms of north-south component ground-velocity motion at TKY015 (a) and CHB014 (b). Corresponding velocity-response spectra for averaged horizontal motions are shown in the right-hand figure. The figures compare the relative excitation strength of the long-period motions for different magnitudes ( $M_w$  7.2, 6.6, 6.0, and 5.4).

saster Mitigation in Urban Areas from the Ministry of Education, Culture, Sports, and Science, Japan. We thank two anonymous reviewers for carefully reading the manuscript. Constructive comments from the reviewers were very valuable for revising manuscript.

Ⓜ Supplementary material comprising MPEG movies for both observed wave propagation and numerical simulation (Figs. 2, 8, and 11) are available in the online edition of BSSA.

## References

- Anderson, J. G., P. Bodin, J. N. Brune, J. Prince, S. K. Singh, R. Quaas, and M. Onate (1986). Strong ground motion from the Michoacan, Mexico earthquake, *Science* **233**, 1043–1049.
- Architectural Institute of Japan (2000). *Damping in Buildings*, Architectural Institute of Japan, Tsukuba, 278 pp. (in Japanese).
- Furumura, T., and L. Chen (2004). Large scale parallel simulation and visualization of 3D seismic wavefield using the Earth Simulator, *Comput. Model. Eng. Sci.* **6**, 143–168.
- Furumura, T., and L. Chen (2005). Parallel simulation of strong ground motions during recent and historical damaging earthquakes in Tokyo, Japan, *Parallel Comput.* **31**, 149–165.
- Furumura, T., B.L.N. Kennett, and K. Koketsu (2003). Visualization of 3D wave propagation from the 2000 Tottori-ken Seibu, Japan, earthquake: observation and numerical simulation, *Bull. Seism. Soc. Am.* **93**, 870–881.
- Guatteri, M., M. Mai, P. Martin, and G. C. Beroza (2004). A pseudo-dynamic approximation to dynamic rupture models for strong ground motion prediction, *Bull. Seism. Soc. Am.* **94**, 2051–2063.
- Hatayama, K., S. Zama, H. Nishi, M. Yamada, and Y. Hirokawa (2004). Long-period strong ground motion and damage to oil storage tanks due to the 2003 Tokachi-oki earthquake, *Zisin* **57**, 83–103 (in Japanese).
- Hayakawa, T., T. Furumura, and Y. Yamanaka (2005). Simulation of strong ground motions caused by the 2004 off the Kii Peninsula earthquakes, *Earth Planets Space* **57**, 191–196.
- Hikima, K., and K. Koketsu (2005). Rupture processes of the 2004 Chuetsu (mid-Niigata prefecture) earthquake, Japan: a series of events in a complex fault system, *Geophys. Res. Lett.* **32**, L18303, doi 10.1029/2005GL023588.
- Kennett, B.L.N., E. R. Engdahl, and R. Buland (1995). Constraints on the velocity structure in the Earth from travel times, *Geophys. J. Int.* **122**, 108–124.
- Kinoshita, S., H. Fujiwara, T. Mikoshiba, and T. Hoshino (1992). Secondary Love waves observed by a strong-motion array in the Tokyo lowlands, Japan, *J. Phys. Earth* **40**, 99–116.
- Koketsu, K., and M. Kikuchi (2000). Propagation of seismic ground motion in the Kanto basin, Japan, *Science* **288**, no. 19, 1237–1239.
- Koketsu, K., K. Hatayama, T. Furumura, Y. Ikegami, and S. Akiyama (2005). Damaging long-period ground motions from the 2003 Mw 8.3 Tokachi-oki, Japan, earthquake, *Seism. Res. Lett.* **76**, no. 1, 67–73.
- Kudo, K., and M. Sakaue (1989). Oil-sloshing in the huge tanks at Niigata due to the Nihonkai-Chubu earthquake of 1983, *Bull. Earthquake Res. Inst. Univ. Tokyo* **59**, 361–382 (in Japanese).
- Liu, H. L., and D. Helmberger (1985). The 23:19 aftershocks of the 15 October 1979 Imperial Valley earthquake: More evidence for an asperity, *Bull. Seism. Soc. Am.* **75**, 689–708.
- Miura, H., and S. Midorikawa (2001). Effects of 3-D deep underground structure on characteristics of rather long-period ground motion: examination in and around Yokohama City, *Zisin* **54**, 381–395 (in Japanese).
- Miyake, H., and K. Koketsu (2005). Long-period ground motions from a large offshore earthquake: the case of the 2004 off the Kii peninsula earthquake, Japan, *Earth Planets Space* **57**, no. 3, 203–207.
- Nakamura, H., and T. Miyatake (2000). An approximate expression of slip velocity time function for simulation of near-field strong ground motion, *Zisin* **53**, 1–9 (in Japanese).
- Nakamura, R., K. Satake, S. Toda, T. Uetake, and S. Kamiya (2003). 3-D Q structure in the Kanto district, in *Program and Abstracts of the Seismological Society of Japan, 2003 Fall Meeting*, 151 (in Japanese).
- Robertson, O. A., J. O. Vlach, and W. W. Symes (1994). Viscoelastic finite-difference modeling, *Geophysics* **59**, 1444–1456.
- Ryoki, K. (1999). Three-dimensional depth structure of the crust and uppermost mantle beneath Southwestern Japan and its regional gravity anomalies, *Zisin* **52**, 51–63 (in Japanese).
- Sekine, S., M. Matsubara, K. Obara, and K. Kasahara (2005). Fine Q structure of the Kanto region derived with NIED Hi-net amplitude data, in *Program and Abstracts of the Seismological Society of Japan, 2005 Fall Meeting*, B009 (in Japanese).
- Shi, H., and S. Midorikawa (1999a). New attenuation relationship for peak ground acceleration and velocity considering effects of fault type and site condition, *J. Struct. Constr. Eng. AIJ* **523**, 63–70 (in Japanese).
- Shi, H., and S. Midorikawa (1999b). Attenuation relationships of peak ground acceleration and velocity considering effects of fault type and site condition, in *Proc. 12th World Conference on Earthquake Engineering*, 532.
- Tanaka, Y., H. Miyake, K. Koketsu, T. Furumura, T. Hayakawa, T. Baba, H. Suzuki, and T. Masuda (2006). The DaiDaiToku integrated model of the velocity structure beneath the Tokyo metropolitan area (2) (abstract), *Japan Geoscience Union Meet. 2006*, S116–P014 (in Japanese).
- Yamada, N., and H. Yamanaka (2003). Comparison of performance of 3D subsurface structural model in southwestern part of the Kanto plain for strong motion simulations, *Zisin* **53**, 313–324 (in Japanese).
- Yamanaka, H., and N. Yamada (2002). Estimation of 3D S-wave velocity model of deep sedimentary layers in Kanto plain, Japan, using microtremor array measurements, *Butsuri-tansa* **55**, 53–65 (in Japanese).

Earthquake Research Institute  
University of Tokyo  
1-1-1 Yayoi, Bunkyo-ku, 113-0032, Japan  
furumura@eri.u-tokyo.ac.jp  
t-haya@eri.u-tokyo.ac.jp

Manuscript received 4 August 2006.